RSC Advances

ROYAL SOCIETY OF CHEMISTRY

www.rsc.org/advances

Journal Name

ARTICLE

Self-Standing polymer-functionalized reduced graphene oxide papers obtained by UV-process

Received 00th January 20xx,
Accepted 00th January 20xx

DOI: 10.1039/x0xx00000x

www.rsc.org/

I. Roppolo[a†], A. Chiappone[a], L. Boggione[b], M. Castellino[a], K. Bejtka[a], C.F. Pirri[a,b], M. Sangermano[b], A. Chiolerio[a]

Graphene based materials are attracting everyday great attentions due to their outstanding properties. Widening their potentialities through synergic effects in conjuction with other materials represents an intriguing challenge in order to obtain lighter and multi-functional composites. In this paper novel self-standing graphene-based paper-like sheets are investigated, obtained by a facile dual step UV-induced process. This method, employing graphene oxide as starting material, allows to obtain polymeric functionalized reduced graphene oxide papers that could be easily handled, featuring improved mechanical and peculiar electrical properties. Mechanical and thermal properties were investigated as well as their electrical response under different stimuli such as temperature and humidity showing remarkable changes under the same

Introduction

Graphene-based polymer composites are one of the most promising emerging class of materials[1, 2]: they are envisaged to be of fundamental importance in energy storage and conversion applications[3-7], electronics[8-10] and sensing[11-14]. An homogeneous dispersion of graphene in polymers and a good interfacial interaction with the matrix still represent the main challenge[2, 15]. Furthermore, interesting aspects arise from the interaction between matrix and filler, and in certain functional application, the interface itself is considered the crucial point[1, 15]. For this reason, the functionalization of graphene with polymeric chains is important to improve compatibility and to feature new synergic properties[15]. Direct graphene functionalization was achieved by covalent bonding[16-22] (e.g. ATRP,[16] dipolar cycloaddiction[21] etc.) or exploiting Van der Waals interactions.[23-29]

Another very promising approach for a large-scale production of polymer-functionalized graphene sheets consists in chemical modification of graphene oxide (GO). [30-32] Generally GO is produced through a well-established oxidative mechanism from graphite,[33] it is commercially available and relatively cheap. [32] This process brings a large number of reactive groups (e.g. carboxylic acids, epoxy groups and hydroxyl groups) on the surface and at the edges of GO sheets which could be used as starting points for chemical reactions or as anchoring points for polymeric chains.[33-35] During the last decades a large number of different methods were proposed both with "grafting to"[36, 37] or "grafting from" [38-40] approaches for the GO functionalization with polymeric chains. However, GO does not feature the outstanding properties of graphene such as high electrical and thermal conductivities.[32, 41] For this reason the simultaneous reduction of graphene oxide to graphene and its functionalization with polymer chains represents an important goal.

Recently, a facile two-step UV-based process for GO reduction toward reduced graphene oxide (RGO) and the simultaneous covalent grafting of initiating moieties at its surface was proposed. This procedure enables the subsequent photo-grafting of a great variety of monomers for graphene surface functionalization.[39, 42]

In the present work we applied the cited method to functionalize reduced graphene oxide with dimethylamino ethyl methacrylate (DMAEMA). This monomer has been proposed for the graphene functionalization for various application domains such as optoelectronics, [43] sensing[44-46] and biomedical devices.[47,48, 49]

By exploiting the attractive properties of poly(dimethyl amino ethyl methacrylate) (PDMAEMA) together with the previously mentioned grafting method we were able to produce easy to handle and self-standing polymer-grafted RGO paper-like sheets. The mechanical and electrical properties of the self-standing materials were then assessed, evidencing the effects induced by the presence of grafted polymer chains.

Experimental

[a] Istituto Italiano di Tecnologia (IIT), Center for Space Human Robotics@Polito, Corso Trento 21, 10129 Torino, Italy.
[b] Department of Applied Science and Technology – DISAT, Politecnico di Torino, C.so Duca degli Abruzzi 24, 10129 Torino, Italy.
† Corresponding Author. Email: Ignazio.roppolo@iit.it

Electronic Supplementary Information (ESI) Sketch of the finctionalization mechanism, FT-IR spectra, XPS survey spectra and N high resolution spectra, TGA and DSC curves, cross-section FESEM images of the samples as prepared and after thermal treatment, IR spectra of the functionalized samples after thermal treatment, video showing the effect on the samples of the humidity.. See DOI: 10.1039/x0xx00000x

Materials

Commercial GO (thickness 0.7–1.2 nm; lateral dimensions 300-800nm) was purchased from Cheap Tubes Inc. (USA) and used without further purification. Benzophenone (BP, Sigma-Aldrich) was used as reducing and anchoring agent. 2-DiMethyl Amino Ethyl Methacrylate (DMAEMA, Sigma-Aldrich) was used as functionalizing monomer. Dimethylformamide DMF and Ethanol were used as solvents.

Functionalization process

The method used in this work was described in details elsewhere.[39] A full scheme of the procedure is reported in Figure S1 in the SI. The amount of each component and the irradiation time were chosen based on previous work.[39, 42] 10 mg of GO in DMF (0.5 mg/ml solution) were placed in a 100 ml three necked flask. The mixture was sonicated in an ultrasound bath until a homogeneous dispersion was obtained. 30 mg of BP powder were then added to the solution, which was magnetically stirred and degassed by bubbling nitrogen for 30 minutes. The mixture was UV irradiated under a high-pressure mercury lamp featuring an intensity of 40 mW/cm^2 (Hamamatsu LC8 equipped with 8 mm light guide) while stirring at room temperature for 5 minutes. Afterwards, the solution was transferred into centrifuge tubes and centrifuged at the speed of 5000 rpm for 10 minutes. The precipitates were then washed with ethanol and centrifuged several times in order to remove the unreacted BP and byproducts. The purified product was dried overnight at 60°C. For the second functionalization step, 10 mg of the modified powder were dispersed in 20 ml of DMF under the presence of different amounts of DMAEMA monomer (50, 150 and 500 mg). The solution was magnetically stirred, degassed by bubbling nitrogen for 30 minutes and subsequently UV irradiated for 90 minutes. The mixture was then centrifuged, washed and dried as previously described in order to eliminate ungrafted polymeric chains. Finally the solution was filtered using a Whatman Anodisc 47 alumina filter (pores diameter 0.1 µm), a self-standing sample (50 µm thickness) was thus obtained after solvent evaporation (1 h at 60°C in vacuum oven).

For comparison in AC electrical measurements a RGO + 500 DMAEMA paper was subjected to a quaternarization process according to literature results that predicted an improvement of moisture sensitivity.[45] Quaternarization process was carried out by laying the membrane 24 h in isopropanol/ ethylene bromide solution (50/50 wt.). The sample was then dried in vacuum oven and tested.

Characterization methods

FT-IR transmittance spectra were collected on a Tensor 27 FTIR Spectrometer (Bruker). The samples were prepared via casting on Si wafer from ethanol. 64 scans were signal-averaged at a resolution of 2 cm^{-1} from 4000 to 400 cm^{-1}.

A PHI 5000 Versaprobe Scanning X-ray Photoelectron Spectrometer (monochromatic Al K-α X-ray source with 1486.6 eV energy, 15 kV voltage and 1 mA anode current), was used to investigate surface chemical composition. A spot size of 100 µm was used in order to collect the photoelectron signal for both the high resolution (HR) and the survey spectra. Different pass energy values were employed: 187.85 eV for survey spectra and 23.5 eV for HR peaks. All samples were analyzed with a combined electron and Argon ion gun neutralizer system in order to reduce the charging effect during the measurements. All core-level peak energies were referenced to C1s peak at 284.5 eV and the background contribution in HR scans was subtracted by means of a Shirley function.[50] Spectra were analysed using Multipak 9.0 dedicated software. Samples were excited with an Ar−Kr laser source (wavelength of 514.5 nm, photon flux ~300 W/cm^2).

Thermogravimetric analysis (TGA) was performed with a Netzsch TG 209 F1 Libra instrument. All samples were previously maintained 30 minutes at 100°C in order to eliminate adsorbed water and then heated between 100°C and 800°C at a heating rate of 10°C/min in nitrogen flow of 60 ml/min. Afterwards a purge flow of nitrogen was used (20 ml/min). For control of the measurements as well as for data acquisition, NETZSCH PROTEUS 32-bit Software was employed with Advanced Software packages like c-DTA (calculated DTA-signal), Super-Res (rate-controlled mass change) and Thermokinetics.

Differential scanning calorimetry (DSC) experiments were performed using a Netzsch DSC 204 F1 Phoenix instrument, equipped with a low temperature probe. The experiments were carried out between 0 and 100 °C with a scan rate of 10 °C/min. For each sample, the same heating module was applied and the final heat flow value recorded during the second heating cycle. The T_g was defined as the midpoint of the heat capacity change observed in the DSC thermogram.

DMTA measurements were performed with a Triton Technology TTDMA. All the experiments were conducted with a temperature ramp of 3°C/min, applying a force with frequency of 1 Hz and with 10 µm of displacement.

Morphologic characterization was performed in top and cross-section views by Field Emission Scanning Electron Microscopy (FESEM, ZEISS Dual Beam Auriga). Cross-section samples were prepared by fracturing them in liquid nitrogen. Prior to FESEM observation samples were coated by a 8 nm thick Pt film via sputtering for improving electrical conductance.

Electrical properties were characterized on free standing membranes at room temperature, using a direct contact setup with stainless steel blocking electrodes, both in DC and in AC regime, up to 2 MHz; the measurements were performed by using a Keithley 2635A multimeter (DC) and an Agilent E4980A precision LCR meter (20 Hz up to 2 MHz).

Results and Discussion

In this work RGO paper-like samples covalently functionalized with different amounts of PDMAEMA using GO as starting materials were synthesized through a UV-mediated two step method previously proposed (Figure S1 in SI). [39]

The process envisages in its first step the UV irradiation of a GO solution in the presence of BP. In fact this latter is known to be able to abstract, under UV irradiation extractable hydrogen atoms from the surrounding, creating semipinacol radicals.[51] It was demonstrated that the BP abstraction of

hydrogen atoms from GO surfaces, which are rich of H-containing groups, induces a spontaneous reduction of GO. Simultaneously, some of the generated semipinacol radicals recombine with latent radicals on the reduced GO surface, inducing the grafting of these molecules.[42]

During the second step these bonds can be homolitically broken through a second UV irradiation, generating an initiating point for the grafting of acrylic and methacrylic monomers.

At the end of this process polymer-functionalized RGO is obtained, featuring polymer brushes grown from the RGO surface. After a washing step (performed in order to get rid of ungrafted chains), self standing functionalized papers were obtained after filtering the solutions, producing easy-to-handle and mechanically robust samples (see Figure 1a).

The presence of grafted polymeric chains on RGO was confirmed by different methods. Figure 1b shows a partial FT-IR spectra of GO, where RGO was reduced in the presence of benzophenone and functionalized with different amounts of DMAEMA (full spectra are reported in SI). In all the samples irradiated in the presence of methacrylic monomers the evidence of C-H stretching peaks around 2900 cm^{-1} is clear. They could be attributed to grafted polymer chains while the same peaks are not present in the pristine GO and in the GO reduced in presence of BP. This measurement clearly shows the presence of polymeric chains grafted on the RGO sheets, however it was not possible to quantify the extent of polymer functionalization, leading to a further experimental search.

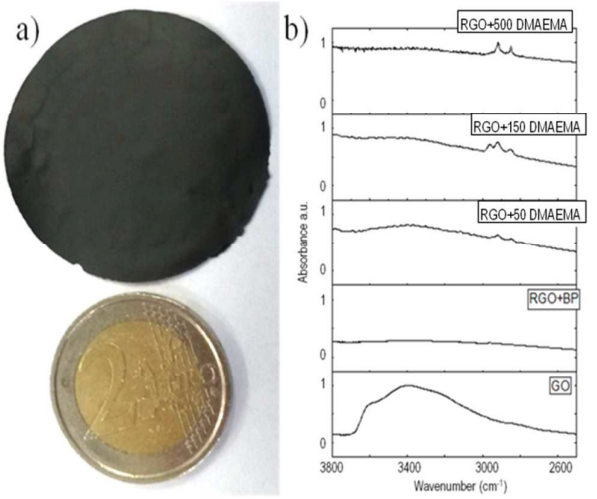

Figure 1 (a) figure of the self-standing RGO paper compared with a 2€ coin (b) IR spectra of the synthesized samples.

XPS measurements were performed in order to better qualify the grafted polymer on the RGO samples. In Figure 2 HR spectra of C1s are reported (see relative survey spectra in SI). Figure 2a reports the starting material (RGO+BP) that shows a high degree of reduction since the peaks relative to C-O (peak 2) and O-C=O (peak 3) represents only the 15.5% of the total area, while the rest is due only to C-(C,H) (peak 1) species. On the other hand, by increasing the amount of DMAEMA in the initial mixture, an increase of peak 2 and peak 3 was observed (Table 1). These peaks can be attributed to an increase in C-(O,N) and O-C=O bonds present in the polymeric chain(Table 1). Moreover it is possible to evidence that N is present only in the sample in which DMAEMA was grafted and an increase of relative abundance of O and N was measured in the samples in which more polymer was grafted. The N1s peak (Figure S11 in SI) is a clear fingerprint of the amine in the DMAEMA monomers. It is made up by the superposition of an higher peak at lower binding energy (peak 1) and a lower peak at higher chemical shift (peak 2). The first component is due to the tertiary amine signal, while the second one is due to the protonated tertiary amine signal.[52] The relative abundance of the two chemical bonds is reported in Figure S12 in SI. While in the RGO+50 and RGO+150 samples the tertiary amine signal is higher and increases with the increase of the initial monomer amount, it is clearly noticeable that in the RGO+500 DMAEMA sample, the protonated amine peak has reached the amine intensity. This can be explained considering that by increasing the amount of polymer grafted on RGO surface increases also the probability of inter-chain H abstraction induced by the amine moiety and thus the amount of protonated tertiary amines.

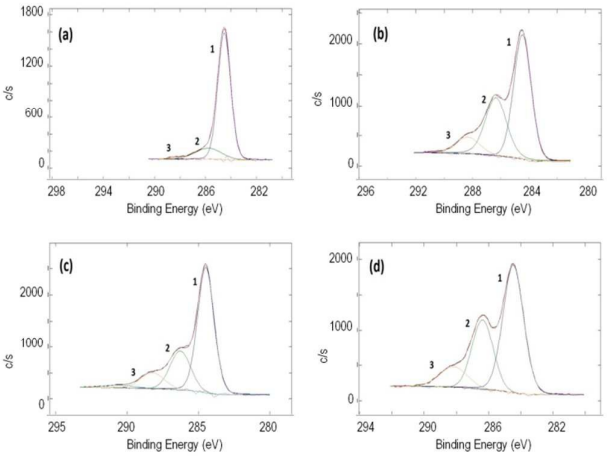

Figure 2 XPS spectra of C1s of (a)RGO+BP, (b) RGO+50 DMAEMA, (c) RGO+150 DMAEMA, (d) RGO+500 DMAEMA

TGA experiments were performed to evaluate the extent of grafting by weight drop, and D-TGA curves are reported in Figure 3. As already demonstrated[39, 42] the peak at 180°C is related to the presence of unreacted semipinacol groups while the second peak at about 350°C is related to the degradation of PDMAEMA polymeric chains (see Figure S11 in SI). It is

evident that, by increasing the amount of monomers, the second peak becomes more intense while the first one decreases. This is an indication that, by increasing the amount of monomers in the formulations, at the end of the second irradiation step a lower amount of unreacted semipinacol radicals remain on RGO sheets and a higher number of polymer chains grow from sheet surfaces. By an evaluation of the weight drop between 200 °C and 450 °C (values between which the polymer undergoes complete thermal degradation) and excluding a measurement drift, it is possible to estimate the amount of polymer grafted. Drop of weight values, reported in Table 2, show that by increasing the amount of monomers in the initial solution a higher degree of polymer functionalization was achieved. However, those values should be taken as an approximation since it is not possible to compare directly the thermal behaviour of neat polymers and of polymeric chains grafted on a surface due to synergic effects during thermal degradation.

The increase of grafted polymer has a clear influence on the thermal behaviour of the free standing RGO papers. Data reported in Table 2 show that a glass transition temperature (T_g) appears evident only in grafted samples and it is more and more evident by increasing the amount of monomers (see SI, Figure S14). This is a further confirmation that increasing the monomer content in the initial solution proportionally scales the grafting degree. Tgs measured in RGO+PDMAEMA samples are higher than those of the neat polymer(54°C, see Figure S16 in SI), indicating that the relaxation of the grafted chains is hindered by the grafting on RGO sheets.

Table 1 XPS relative atomic concentration of C, O and N elements (data taken from the survey spectra) and C1s chemical shifts relative concentration (from C1s deconvolution procedures).

Sample	Atomic %			C1s		
	C	O	N	C-(C,H)	C-(O,N)	O-C=O
RGO+BP	85.8	14.2	-	84.5	14.5	1.0
RGO+50DMAEMA	72.4	25.5	2.1	55.6	33.9	10.5
RGO+150DMAEMA	70.3	27.0	2.7	64.5	24.3	11.2
RGO+500DMAEMA	68.1	29.0	2.9	57.2	30.8	12.0

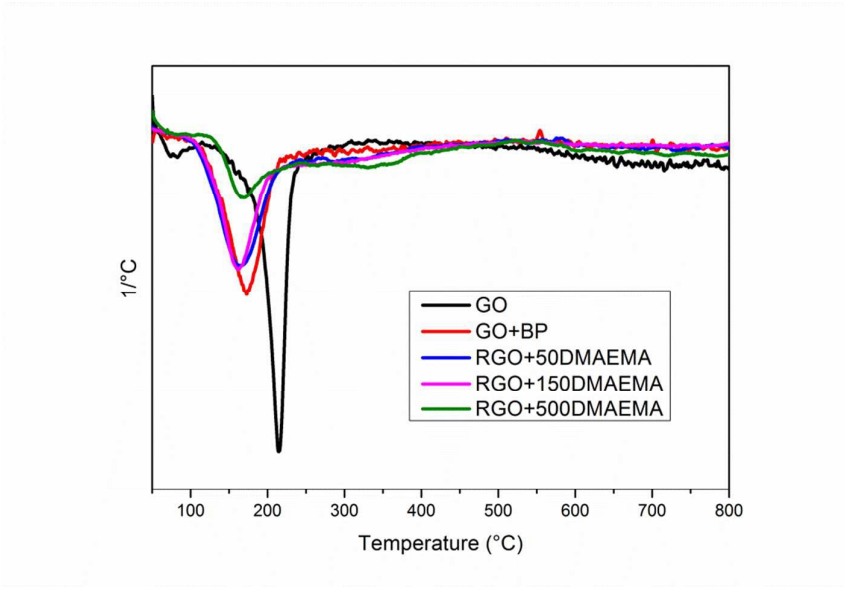

Figure 3 D-TGA for GO, RGO+BP and RGO with different amounts of DMAEMA

Table 2 Thermal characteristics of the synthesized samples

Sample	T_{degr1} [°C]	T_{degr2} [°C]	Polymer drop of weight [%]	T_g (DSC) [°C]	$T_{slipping}$ (DMTA) [°C]
RGO+BP	172	-	-	-	-
RGO+50DMAEMA	162	334	3	64	18
RGO+150DMAEMA	162	334	5	75	50
RGO+500DMAEMA	168	334	7.5	65	60

The higher amount of grafted polymer chains has an important influence on the mechanical properties of RGO papers. First of all, macroscopically, after grafting the RGO papers result easier to handle and quite robust while GO and RGO+BP papers are brittle and difficult to manipulate. To better quantify this property, DMTA measurements were performed. In Figure 4 DMTA curves for samples produced after the filtering step are showed. It is clear that both GO and RGO+BP papers present very poor mechanical properties ($E'_{GO} = 2$ MPa, $E'_{RGO+BP} = 4$ MPa), related to simple secondary force interactions between GO or RGO sheets. Those values are stable to temperature variation, confirming the absence of any transition measured by DSC. For the sample grafted with PDMAEM an increase of mechanical properties at low temperature was found ($E'_{RGO+50DMAEMA} = 15$ MPa, $E'_{RGO+150DMAEMA} = 40$ MPa, $E'_{RGO+500DMAEMA} = 130$ MPa), showing the positive influence of the polymer grafting on the mechanical properties.[53] Those E' values make our paper compatible with applications such as artificial skin, which is of particular interest in certain robotic frameworks.[53] At higher temperatures, an important decrease of the storage moduli is also found for all these samples. Those transition values ($T_{slipping}$ in Table 2) could be seen as the temperatures at which the grafted polymer chains have enough mobility to disentangle and thus slip, reaching E' values comparable with unfunctionalized papers. This means that at temperatures lower than $T_{slipping}$ the papers' mechanical response is controlled by interchain interactions while at higher temperatures only secondary forces are operating. This transition occurs at higher temperatures by increasing the amount of grafted polymer chains, this could be explained considering that the higher is the amount of polymer chains (and their length too) the higher is the temperature necessary to disentangle them. $T_{slipping}$ values are quite different from T_gs measured in DSC but it must be taken into account that the two measurements are based upon the evaluation of different properties. While DSC measures differences in the heat absorbance, DMTA evaluates mechanical properties under a sinusoidal force. So, as previously mentioned, $T_{slipping}$ could be seen as the temperature at which the chains grafted on RGO sheets disentangle and not as the T_g of the material. On the other hand the T_gs measured with DSC could be considered more similar to the final typical moduli decrease at temperatures higher than 85 °C, when a typical polymer flow occurs.

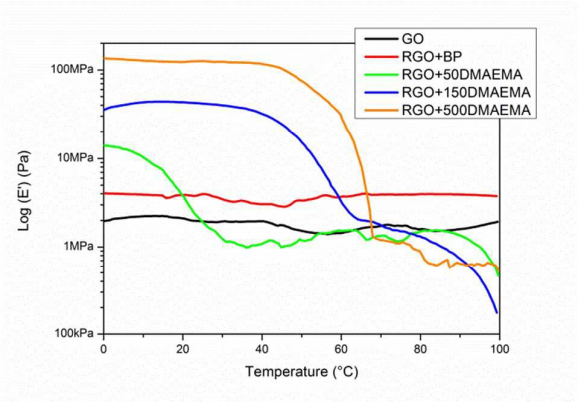

Figure 4 E' DMTA curves obtained for free standing samples

The presence of polymeric chains is particularly evident by observing top view and cross-section FESEM images, shown in Figure 5 and Figure S17 in SI, respectively. The pristine RGO+ BP (Figure 5a) shows mostly wrapped flakes resulting in rough surfaces, while in the presence of polymer (Figure 5b) the surface appears smoother. This is an indication that polymeric chains completely cover the sheets and help them to extend smoothly. When the content of polymer chains is further increased polymeric aggregation occurs on the surface of the sheets, resulting in white particles on the surface. Moreover it is possible to foresee that the presence of polymeric chains increases the distance between RGO sheets (see membrane cross-section images in Figure S17 in SI). This is in agreement with DMTA studies in which the effect of the presence of polymeric chains on the mechanical properties of the papers was demonstrated.

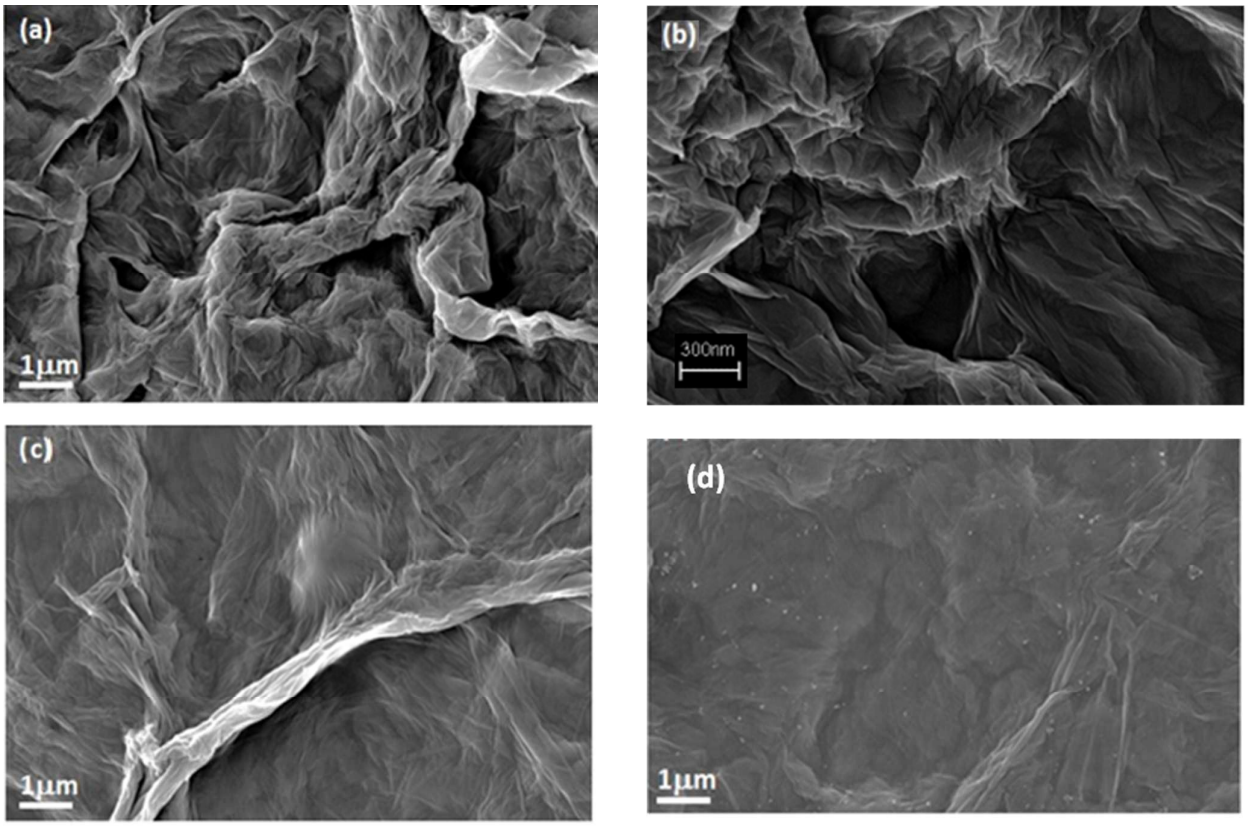

Figure 5 FESEM images of (a) RGO+BP, (b) RGO+50 DMAEMA and (c) RGO+500DMAEMA

Electrical characterization

Electrical measurements were performed on graphene membranes using the two point contact method in order to assess any interface effect due to the presence of polymeric chains (Figure 6a). It was observed that the conductivity of the RGO+BP paper results enormously lower than the conductivity of the single RGO+BP sheet (13 S/cm).[39] This may be expected considering that the conductivity of the whole material is affected by sheet to sheet contact resistance, in other words by the difficult inter-sheet hopping of charges. [54] Moreover it is evident that increasing the amount of polymer grafted on the sheets strongly affects the electrical conductivity, decreasing σ by 3 orders of magnitude with respect to the RGO+BP. This is in good agreement with our previous evaluation: the presence of a polymeric chain on the graphene sheets further increases the distance between the sheets and thus decreases the conductivity.

In order to assess the effect of the temperature on the polymer grafted RGO papers, samples were firstly heated to different temperatures up to 110°C and then tested at room temperature. With this approach the effect of a thermal treatment on the papers was evaluated. RGO+BP paper conductivity is not strongly affected by the thermal treatments (see Figure S17 in SI) while in the presence of polymer chains the conductivity increases by more than one order of magnitude. This could be explained considering that by increasing the temperature at $T > T_g$, polymer chains could undergo a relaxation and thus a higher hopping probability could be induced in the samples, according to a mechanism that we propose in Figure 7. The comparison between cross-section images of papers before (see Figure S18 SI) and after thermal treatment (Figure S19 in SI) in fact confirms that the latter are more closely-packed, indicating a reduction of the distance between the RGO sheets. Subsequently, FTIR experiments were performed on the tested samples in order to investigate whether polymeric chains were degraded or not after thermal treatment. The graphs (reported in Figure S20 in SI) confirm the presence of polymeric chains at any temperature, indicating that the structures were preserved.

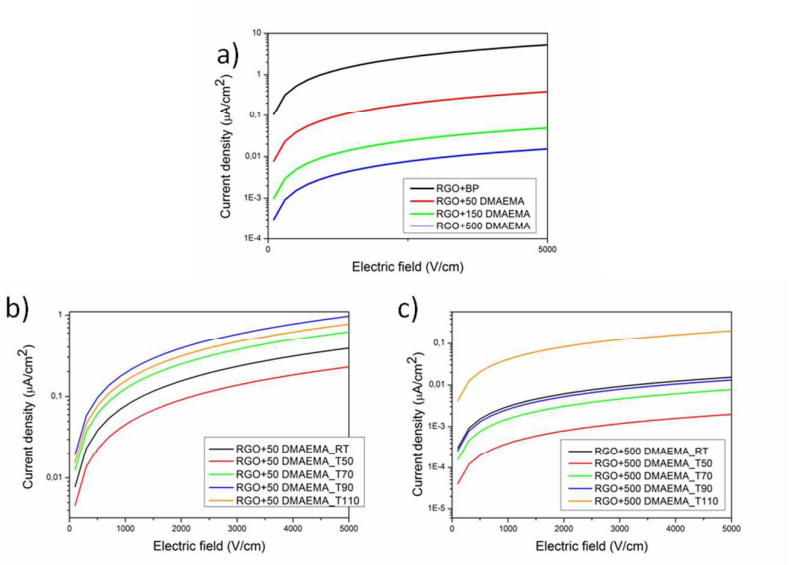

Figure 6 I-V curves of the synthesized materials at room temperature (a), I-V curves collected after thermal treatments at different temperatures for RGO+ 50 DMAEMA (b) and RGO +500 DMAEMA (c)

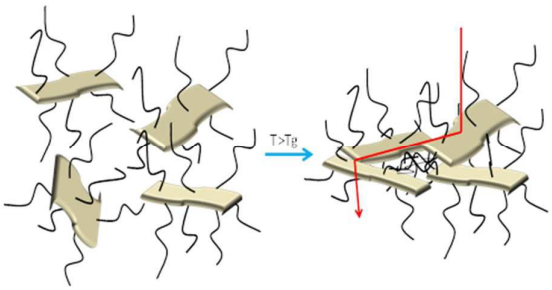

Figure 7 Mechanism proposed for explanation of the electrical behaviour of the polymer functionalized RGO paper samples

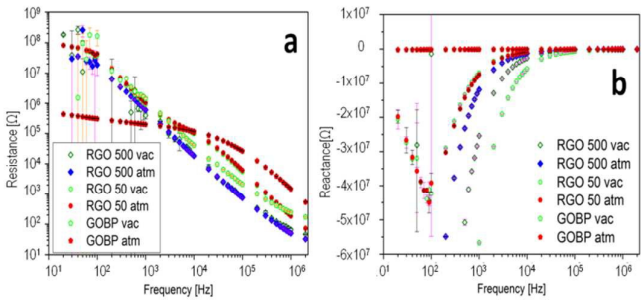

Figure 8 Impedance spectroscopy measurements in the range 20 Hz – 2 MHz at room temperature, resistance (panel a) and reactance (panel b) versus frequency.

AC electrical measurements were also performed on two families of samples: standard samples kept always in room conditions and vacuum-dried ones (overnight in a vacuum oven to remove adsorbed moisture). Figure 8 shows the impedance spectroscopy measurements (panel a: resistance; panel b: reactance), for all tested samples. Sample RGO + 500 DMAEMA shows no remarkable difference between the measure after exposure to either vacuum (RGO 500 vac sample) or to standard atmosphere (25 % RH, RGO 500 atm sample). Sample RGO + 50DMAEMA also shows overlapping impedance responses, in both conditions. GO+BP features a response very similar to the other samples when subject to vacuum. However, when subject to standard atmosphere, its conductivity is much higher in the low frequency regime (below 1 kHz) and slightly lower in the high frequency regime (above 10 kHz).

To better understand the frequency response of the most relevant samples (GO+BP, the one with the highest amount of polymer RGO+500DMAEMA and a sample submitted to quaternarization process), we propose a comparison between the Nyquist plots in bilogarithmic scale (Figure 9a), summarizing the impedance curve in one single plane. Two curves are compared for each material: one recorded after exposure to primary vacuum-drying and one after exposure to standard atmosphere (40 % R.H.). We tested the membranes with two signals, one featuring a small amplitude (100 mV) and another one featuring a higher rms (1 V); since there were no relevant differences we show only the 1 V-related measurements, featuring lower noise. Removal of water results in a different conduction mechanism, depending on the tested material. Impedance locus evolution is such that we do not see anymore the diffusive part (change in slope appearing

at frequencies in the kHz regime (red dots), standard atmosphere with 40 % R.H.) and we just see the capacitance associated to the membrane (that is the single sloppy line). This means that humidity in the GO+BP membrane provides a mechanism for the diffusion of charge carriers, without which no more diffusion occurs. In the case of RGO + 500 DMAEMA we have a reversed mechanism, since the change in slope associated to the diffusive part is only seen when moisture is present in the film. Furthermore an extremely interesting property was found: in the kHz regime the two responses overlap, providing a clue for practical applications: by spanning the frequency range from this point on, one may find an impedance modulus much reduced as a function of the signal frequency. All other responses show a more constant difference, which is not depending on the frequency. We find the greatest difference between the two electronic states of RGO + 500 DMAEMA at 2 MHz, suggesting that we are not simply looking into the ionic conduction channel, but rather on a structural difference induced by water molecules. Finally a RGO + 500 DMAEMA sample after quaternarization process is proposed, showing that we recover the same phenomenology of the GO + BP paper, with a much lower intensity with respect to the same sample before quaternarization. In conclusion, fixing the signal frequency to 1 MHz as example, we will find that: GO + BP shows a difference between dry conditions and 40% R.H. of one order of magnitude in resistance and .3 orders of magnitude in reactance; RGO + 500 DMAEMA shows a difference of one order of magnitude both in resistance and reactance (best performance); RGO + 500 DMAEMA after quaternarization process shows no difference in resistance and .1 orders of magnitude in reactance.

We can thus conclude that the presence (absence) of moisture affects AC response at frequencies above a threshold value, comprised between 10 Hz and 2 MHz, hindering (enhancing) the conductive and admittive components of impedance, in other words moisture entraps some ions excluding them from transport. This only happens in polymer-grafted papers, as in RGO+BP the effect is reversed and the presence of moisture helps conduction between adjacent sheets.

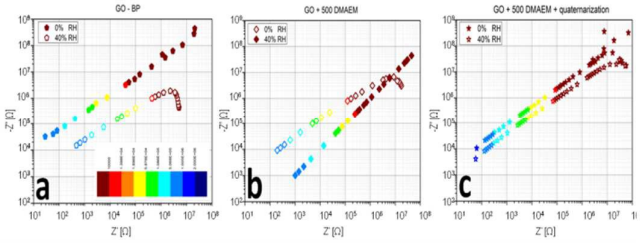

Figure 9: Nyquist plots of a RGO+BP (a), RGO + 500 DMEAM (b) and same as b after quaternarization process (c) membranes in response to humidity variations.

The effect of humidity on the functionalized RGO papers presents also a huge consequence at macroscopic scale: holding a sample in a hand induces an immediate folding, similarly to other works present in literature.[55] This effect is isotropic since it can be reproduced by turning the paper on the other side and is completely reversible in a short time. This effect can be better visualized in the video reported in the Supporting Informations.

Conclusions

In this work self-standing RGO papers were obtained by means of UV-irradiation, applying a two step process leading both to an extensive reduction of pristine GO and to its covalent functionalization with DMAEMA. The grafting was demonstrated to have great influence on mechanical and electrical properties of the synthesized samples. The functionalized papers showed improved mechanical properties, making these materials easy to handle, contrary to the pure RGO samples. Moreover, by DMTA experiments, the behaviour of the papers was demonstrated to be dependent on the amount of polymer grafting, showing a thermoplastic-like behaviour for the samples whit the highest degree of functionalization. The degree of functionalization influences also the electrical response of the papers: samples featuring a higher amount of polymer show very insulating behaviour, with a conductivity three orders of magnitude lower than the corresponding neat RGO sample. On the other side, polymer functionalized samples showed an electrical response depending on the environmental conditions, exhibiting different conductivities after different thermal treatments and a mechanical response to humidity.

References

1. S. Stankovich, D. A. Dikin, G. H. B. Dommett, K. M. Kohlhaas, E. J. Zimney, E. A. Stach, R. D. Piner, S. T. Nguyen and R. S. Ruoff, *Nature*, 2006, **442**, 282-286.
2. V. Georgakilas, M. Otyepka, A. B. Bourlinos, V. Chandra, N. Kim, K. C. Kemp, P. Hobza, R. Zboril and K. S. Kim, *Chemical Reviews*, 2012, **112**, 6156-6214.
3. C. X. Guo, M. Wang, T. Chen, X. W. Lou and C. M. Li, *Advanced Energy Materials*, 2011, **1**, 736-741.
4. X. Jiang, Y. Cao, P. Li, J. Wei, K. Wang, D. Wu and H. Zhu, *Materials Letters*, 2015, **140**, 43-47.
5. C. Liu, Z. Yu, D. Neff, A. Zhamu and B. Z. Jang, *Nano Letters*, 2010, **10**, 4863-4868.
6. Z. Song, T. Xu, M. L. Gordin, Y.-B. Jiang, I.-T. Bae, Q. Xiao, H. Zhan, J. Liu and D. Wang, *Nano Letters*, 2012, **12**, 2205-2211.
7. Q. Wu, Y. Xu, Z. Yao, A. Liu and G. Shi, *ACS Nano*, 2010, **4**, 1963-1970.
8. G. Eda, G. Fanchini and M. Chhowalla, *Nat Nano*, 2008, **3**, 270-274.
9. G. Eda and M. Chhowalla, *Nano Letters*, 2009, **9**, 814-818.

10. S. Porro, E. Accornero, C. F. Pirri and C. Ricciardi, *Carbon*, 2015, **85**, 383-396.
11. A. Zopfl, M.-M. Lemberger, M. Konig, G. Ruhl, F.-M. Matysik and T. Hirsch, *Faraday Discussions*, 2014, **173**, 403-414.
12. H. J. Salavagione, A. M. Diez-Pascual, E. Lazaro, S. Vera and M. A. Gomez-Fatou, *Journal of Materials Chemistry A*, 2014, **2**, 14289-14328.
13. L. Al-Mashat, K. Shin, K. Kalantar-zadeh, J. D. Plessis, S. H. Han, R. W. Kojima, R. B. Kaner, D. Li, X. Gou, S. J. Ippolito and W. Wlodarski, *The Journal of Physical Chemistry C*, 2010, **114**, 16168-16173.
14. Y. Shao, J. Wang, H. Wu, J. Liu, I. A. Aksay and Y. Lin, *Electroanalysis*, 2010, **22**, 1027-1036.
15. T. Kuila, S. Bose, A. K. Mishra, P. Khanra, N. H. Kim and J. H. Lee, *Progress in Materials Science*, 2012, **57**, 1061-1105.
16. M. Fang, K. Wang, H. Lu, Y. Yang and S. Nutt, *Journal of Materials Chemistry*, 2009, **19**, 7098-7105.
17. S. Niyogi, E. Bekyarova, M. E. Itkis, H. Zhang, K. Shepperd, J. Hicks, M. Sprinkle, C. Berger, C. N. Lau, W. A. deHeer, E. H. Conrad and R. C. Haddon, *Nano Letters*, 2010, **10**, 4061-4066.
18. T. A. Strom, E. P. Dillon, C. E. Hamilton and A. R. Barron, *Chemical Communications*, 2010, **46**, 4097-4099.
19. S. Vadukumpully, J. Gupta, Y. Zhang, G. Q. Xu and S. Valiyaveettil, *Nanoscale*, 2011, **3**, 303-308.
20. J. Choi, K.-j. Kim, B. Kim, H. Lee and S. Kim, *The Journal of Physical Chemistry C*, 2009, **113**, 9433-9435.
21. M. Quintana, K. Spyrou, M. Grzelczak, W. R. Browne, P. Rudolf and M. Prato, *ACS Nano*, 2010, **4**, 3527-3533.
22. L.-H. Liu, M. M. Lerner and M. Yan, *Nano Letters*, 2010, **10**, 3754-3756.
23. Y. Wang, X. Chen, Y. Zhong, F. Zhu and K. P. Loh, *Applied Physics Letters*, 2009, **95**, 063302.
24. V. K. Kodali, J. Scrimgeour, S. Kim, J. H. Hankinson, K. M. Carroll, W. A. de Heer, C. Berger and J. E. Curtis, *Langmuir*, 2011, **27**, 863-865.
25. X. An, T. W. Butler, M. Washington, S. K. Nayak and S. Kar, *ACS Nano*, 2011, **5**, 1003-1011.
26. M. Lopes, A. Candini, M. Urdampilleta, A. Reserbat-Plantey, V. Bellini, S. Klyatskaya, L. Marty, M. Ruben, M. Affronte, W. Wernsdorfer and N. Bendiab, *ACS Nano*, 2010, **4**, 7531-7537.
27. H.-C. Cheng, R.-J. Shiue, C.-C. Tsai, W.-H. Wang and Y.-T. Chen, *ACS Nano*, 2011, **5**, 2051-2059.
28. Q. Su, S. Pang, V. Alijani, C. Li, X. Feng and K. Müllen, *Advanced Materials*, 2009, **21**, 3191-3195.
29. W. Tu, J. Lei, S. Zhang and H. Ju, *Chemistry – A European Journal*, 2010, **16**, 10771-10777.
30. H. Yang, F. Li, C. Shan, D. Han, Q. Zhang, L. Niu and A. Ivaska, *Journal of Materials Chemistry*, 2009, **19**, 4632-4638.
31. Z. Liu, J. T. Robinson, X. Sun and H. Dai, *Journal of the American Chemical Society*, 2008, **130**, 10876-10877.
32. D. R. Dreyer, S. Park, C. W. Bielawski and R. S. Ruoff, *Chemical Society Reviews*, 2010, **39**, 228-240.
33. W. S. Hummers and R. E. Offeman, *Journal of the American Chemical Society*, 1958, **80**, 1339-1339.
34. H. Li and C. Bubeck, *Macromolecular Research*, 2013, **21**, 290-297.
35. A. Badri, M. R. Whittaker and P. B. Zetterlund, *Journal of Polymer Science, Part A: Polymer Chemistry*, 2012, **50**, 2981-2992.
36. M. Steenackers, A. M. Gigler, N. Zhang, F. Deubel, M. Seifert, L. H. Hess, C. H. Y. X. Lim, K. P. Loh, J. A. Garrido, R. Jordan, M. Stutzmann and I. D. Sharp, *Journal of the American Chemical Society*, 2011, **133**, 10490-10498.
37. L. Kan, Z. Xu and C. Gao, *Macromolecules*, 2010, **44**, 444-452.
38. S. H. Lee, D. R. Dreyer, J. An, A. Velamakanni, R. D. Piner, S. Park, Y. Zhu, S. O. Kim, C. W. Bielawski and R. S. Ruoff, *Macromolecular Rapid Communications*, 2010, **31**, 281-288.
39. I. Roppolo, A. Chiappone, K. Bejtka, E. Celasco, A. Chiodoni, F. Giorgis, M. Sangermano and S. Porro, *Carbon*, 2014, **77**, 226-235.
40. Y. Yang, J. Wang, J. Zhang, J. Liu, X. Yang and H. Zhao, *Langmuir*, 2009, **25**, 11808-11814.
41. A. K. Geim and K. S. Novoselov, *Nat Mater*, 2007, **6**, 183-191.
42. I. Roppolo, A. Chiappone, S. Porro, M. Castellino and E. Laurenti, *New Journal of Chemistry*, 2015, **39**, 2966-2972.
43. A. Kuila, N. Maity, R. K. Layek and A. K. Nandi, *Journal of Materials Chemistry A*, 2014, **2**, 16039-16050.
44. J. Wang, D. Song, S. Jia and Z. Shao, *Reactive and Functional Polymers*, 2014, **81**, 8-13.
45. Y. Li, Y. Chen, C. Zhang, T. Xue and M. Yang, *Sensors and Actuators B: Chemical*, 2007, **125**, 131-137.
46. S. Gupta, M. Agrawal, M. Conrad, N. A. Hutter, P. Olk, F. Simon, L. M. Eng, M. Stamm and R. Jordan, *Advanced Functional Materials*, 2010, **20**, 1756-1761.
47. Y. Q. Yang, B. Zhao, Z. D. Li, W. J. Lin, C. Y. Zhang, X. D. Guo, J. F. Wang and L. J. Zhang, *Acta Biomaterialia*, 2013, **9**, 7679-7690.
48. D. Lin, Q. Jiang, Q. Cheng, Y. Huang, P. Huang, S. Han, S. Guo, Z. Liang and A. Dong, *Acta Biomaterialia*, 2013, **9**, 7746-7757.
49. S. Maji, F. Mitschang, L. Chen, Q. Jin, Y. Wang and S. Agarwal, *Macromolecular Chemistry and Physics*, 2012, **213**, 1643-1654.
50. D. A. Shirley, *Physical Review B*, 1972, **5**, 4709-4714.
51. H. Ma, R. H. Davis and C. N. Bowman, *Macromolecules*, 1999, **33**, 331-335.
52. N. Graf, E. Yegen, T. Gross, A. Lippitz, W. Weigel, S. Krakert, A. Terfort and W. E. S. Unger, *Surface Science*, 2009, **603**, 2849-2860.
53. A. Chiolerio, P. Rivolo, S. Porro, S. Stassi, S. Ricciardi, P. Mandracci, G. Canavese, K. Bejtka and C. F. Pirri, *RSC Advances*, 2014, **4**, 51477-51485.
54. D. Yu and L. Dai, *Journal of Physical Chemistry Letters*, 2010, **1**, 467-470.
55. D.-D. Han, Y.-L. Zhang, H.-B. Jiang, H. Xia, J. Feng, Q.-D. Chen, H.-L. Xu and H.-B. Sun, *Advanced Materials*, 2015, **27**, 332-338.